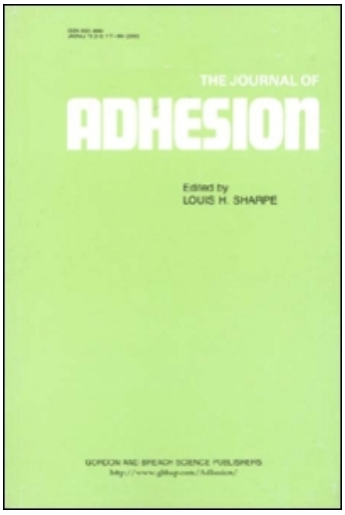

The Journal of Adhesion
Publication details, including instructions for authors and subscription information:
http://www.informaworld.com/smpp/title~content=t713453635

Modulation of Adhesion at Silicone Elastomer-Acrylic Adhesive Interface

L. Léger[a]; N. Amouroux[a]
[a] Laboratoire de Physique des Fluides Organisés, UMR CNRS, Collège de France, Paris, France

To cite this Article Léger, L. and Amouroux, N.(2005) 'Modulation of Adhesion at Silicone Elastomer-Acrylic Adhesive Interface', The Journal of Adhesion, 81: 10, 1075 — 1099
To link to this Article: DOI: 10.1080/00218460500310812
URL: http://dx.doi.org/10.1080/00218460500310812

The Journal of Adhesion, 81:1075–1099, 2005

ISSN: 0021-8464 print/1545-5823 online
DOI: 10.1080/00218460500310812

Taylor & Francis
Taylor & Francis Group

Modulation of Adhesion at Silicone Elastomer–Acrylic Adhesive Interface

L. Léger
N. Amouroux
Laboratoire de Physique des Fluides Organisés, UMR CNRS, Collège de France, Paris, France

To characterize the role of small silica like nanoparticles (MQ resins) in the modulation of adhesion at polydimethyl siloxane (PDMS) elastomers–acrylic adhesive contacts, we have designed systems in which the roles of MQ resins in enhancing interactions at the interface and in increasing viscoelastic dissipations in the elastomer layer could be separated. First, the contact between elastomers with various MQ resin contents and PDMS layers made of densely grafted short chains has been investigated through Johnson–kendall–Roberts (JKR) tests, in order to characterize how the dissipations in the elastomer depend on the resin content. The same elastomers in contact with thin-surface-anchored acrylic layers were then tested through JKR tests to determine the role of enhanced interactions in the modulation of adhesion at the interface due to the resins. In these experiments, the thickness of the acrylic layer was kept small enough so that dissipations in the acrylic adhesive could be neglected. Both G_0, the adhesive strength at zero fracture velocity, and $G(V)$, the velocity-dependent fracture toughness, strongly depend on the MQ resin content and on the contact time, suggesting the progressive building of strong interactions between acrylic and elastomer chains.

Keywords: Acrylic adhesives; Adhesion mechanisms; Dissipation; Interfacial interactions; JKR test; Silicone elastomers

Received 1 March 2005; in final form 23 July 2005.

One of a collection of papers honoring Manoj K. Chaudhury, the February 2005 recipient of The Adhesion Society Award for Excellence in Adhesion Science, sponsored by 3M.

Address correspondence to Liliane Léger, Laboratoire de Physique des Fluides Organisés, UMR CNRS, Collège de France, 11 Place Marcelin Berthelot, 75231 Paris Cedex 05, France. E-mail: liliane-leger@college-de-france.fr

INTRODUCTION

In a number of weakly adhering systems, it is desirable to precisely adjust the level of adhesion, as for example in repositionable devices, for which one may wish to easily peel apart the two partners, while still avoiding spontaneous delamination. This can be achieved by using silicone elastomer coatings in contact with acrylic adhesives, the silicone elastomers being chemically modified by incorporation of silicone MQ resins (small silica-like nanoparticles) to adjust the level of adhesion. It is commonly assumed that the role of the MQ resins is to enhance interfacial interactions, because of their slightly higher polarity compared with pure silicone elastomer. To better identify and understand the molecular mechanisms involved in such modulation of adhesion, we have undertaken a systematic investigation of the respective roles of interfacial interactions and bulk dissipations in fixing the level of adhesion at silicone elastomer–acrylic adhesive interfaces. We present here the first part of this work, in which the adhesion between bulk silicone elastomers containing various amounts of MQ resins and a commercial acrylic adhesive is characterized through the well-known JKR test.

We first present the materials, the JKR test apparatus, and the experimental protocols we have used to characterize adhesive strength. Results for silicone–silicone contacts are then presented and compared with results obtained for silicone microlenses containing variable amounts of MQ resins in contact with a molecularly thin layer of acrylic adhesive deposited on silicon wafers. The thickness of this adhesive layer is chosen to be small enough to ensure that dissipations in the adhesive layer do not contribute significantly to the measured adhesive strength. The effect of changing the physicochemical interactions at the interface by progressively increasing the MQ resin content in the silicone elastomer can then be isolated and identified. We have also investigated in a systematic manner how these interactions produce adhesion by using the same elastomer lenses in contact with self-assembled monolayers of end-functionalized thiol molecules. The exact nature and the number of the functional groups present at the interface are then under control. These experiments on controlled substrates of various chemical compositions will be presented in a forthcoming paper, along with results obtained on the reverse system (with the elastomer lens made of a crosslinked acrylic polymer very similar to conventional acrylic adhesives and put into contact with a thin PDMS or MQ resin layer). The full series of experiments allow one to separate the relative contributions to adhesive strength of the dissipations

in the silicone layer and in the adhesive layer, as a function of the interactions at the interface. In the present article, we focus our attention on the contact between thick silicone elastomer/thin acrylic layer on a rigid substrate.

MATERIALS AND EXPERIMENTAL TECHNIQUES

The synthesis and the characteristics of the silicone elastomers used in the present study have already been reported [1, 2]. We briefly summarize here their main properties.

Silicone Substrates

Silicone elastomers were prepared using polydimethylsiloxane (PDMS) and MQ silicone resins in various proportions. The divinyl-terminated PDMS ($M_n = 17000$ g/mol by titration, $I = M_w/M_n = 1.3$ by gel permeation chromatography) was obtained after several precipitations in acetone of a commercial-grade silicone oil (Rhodia 621V200, Rhodia Silicone, Saint Fous, France). The silicone $MD^{Vi}Q$ resin (Rhodia) was used as received. Its chemical composition was estimated using ^{29}Si NMR ($M = Me_3SiO_{1/2}$:47.3 wt%, $D^{Vi} = ViMeSiO_{2/2}$:9.1 wt%, $Q = SiO_{4/2}$: 43.6 wt%). The ratio O/Me is close to unity, and, thus the resin is expected to be less apolar than PDMS, which has two methyl groups for one oxygen. From small-angle x-ray scattering experiments we know that the resin particles have compact structures with radii of gyration $R_g = 1$–2 nm. The corresponding average molecular mass is in the range 3000–5000 g/mol. Blends of PDMS and resin (0 wt% up to 40 wt% in resin) were prepared, and the concentration of vinyl groups was titrated. The catalyst (Karstedt's Pt) is added using 20 ppm of Pt for 10^{-4} mol of vinyl groups. After addition of 1,3,5,7 tetramethyltetracyclosiloxane (D′4), which acts as a tetra functional crosslinker, the mixture is stirred for 15 min, degassed, and then deposited on fluorinated glass slides to form small spherical caps, following the technique first introduced by Chaudhury and whitesides [3]. In the case of the mixture without $MD^{Vi}Q$, the pot life at ambient temperature is short; therefore, the stirring after addition of D′4 is performed at –15°C under a dry nitrogen atmosphere. The samples are cured overnight at 100°C. The relative quantity of D′4 is adjusted to minimize the sol fraction ($r = [SiH]/[C{=}C] = 1.2$ for pure PDMS and $r = 1.7$, 1.8, 1.95, and 2.2 for 10, 20, 30, and 40 wt% resin, respectively). Thick ribbons of the same elastomers are also formed simultaneously and used either to test the mechanical properties of the elastomers or to prevent finite-size effects in the JKR test [4]. Dynamic

mechanical properties were probed with a Rheometrics RSAII solid analyzer at 25°C using thick ribbons (1 mm) (TA Instruments Rheometrics, Guyancourt, France). Surface energies were characterized by dynamic tensiometry using H_2O and tricresylphosphate. The storage and loss moduli of the different elastomers used have been reported in [1]. The storage moduli, E', increase from 8.10^5 Pa for pure PDMS elastomers up to 6.10^6 Pa for an elastomer filled with 40% (by weight) of MQ resin. The loss moduli, E'', increase much more, gaining three decades between small resin content ($\sim 10^3$ Pa) and 40 wt% resin content ($\sim 10^6$ Pa). All elastomers remain, however, essentially elastic because $tg\delta = E''/E'$ remains smaller than 0.1.

In contrast to bulk mechanical properties, the surface energies appear independent of the resin content. The dispersive component of surface energy is equal to $\gamma^D = 21 \pm 1$ mN/m for all samples, whereas the nondispersive component slightly increases from $\gamma^{ND} \approx 0$ to 2 ± 1 mN/m between 0% and 40% resin content.

JKR Test

Two JKR machines schematically presented in Figure 1 have been used. They are quite similar to that described in Reference [4], except for the motorization of the rigid holder of the small elastomer lens, using a step-by-step motor. The rigidity constants of the force sensors

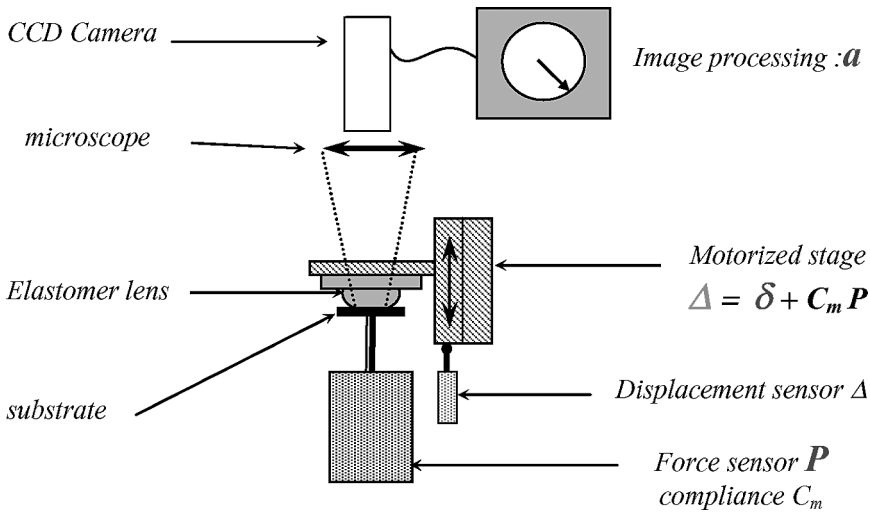

FIGURE 1 Schematic representation of the JKR apparatus.

are $k = 219$ or $256\,\mathrm{N/m}$, respectively. The displacement $\triangle$ of the lens holder, imposed by the motor, is measured through a linear variable differential transformer (LVDT) displacement sensor. The contact area between the elastomer lens and the substrate is monitored through a CCD (coupled charge device) camera and analyzed online through image analysis software that we have developed. The apparatus allows one to measure simultaneously the radius of the contact area, $a(t)$, the load, $P(t)$, and the displacement $\delta(t)$, or deformation of the lens at the center of the contact. From a and P, the adhesive strength G can be deduced through the JKR analysis [5, 6] as a function of the velocity of the contact line, V. The simultaneous measurement of the displacement δ allows one to test the validity of the JKR analysis. All JKR measurements are performed in two steps: loading and unloading.

Loading

During the loading step, the lens is first slowly brought down to the substrate to establish the contact. Then, small steps in displacement Δ (0.5 to 2 μm) are applied at chosen time intervals.

The elastic modulus of the lens, K, and the adhesive strength, G, can be deduced by fitting the data to the JKR equation,

$$a^3 = \frac{R}{K}\left[P + 3\pi GR + \sqrt{6\pi GRP + (3\pi GR)^2}\right], \tag{1}$$

with R as the radius of the lens. If the loading speed is chosen slow enough so that the contact reaches equilibrium at each step, but rapid enough so that only instantaneous Van der Waals forces are able to develop under contact, the adhesive strength can be identified as the thermodynamic work of adhesion, W.

The JKR Equation (1) can be rewritten in the linear form:

$$\frac{P}{\sqrt{6\pi a^3}} = K\frac{a^{3/2}}{R\sqrt{6\pi}} - \sqrt{GK}. \tag{2}$$

In Figure 2, a typical example of such a loading curve analyzed in terms of either Equation (1) (Figure 2a) or Equation (2) (Figure 2b) is reported for a situation where the JKR analysis holds (silicone elastomer against the same elastomer) as demonstrated by the straight line in Figure 2b.

Unloading

After a given waiting time under the maximum load, the unloading is performed by steps, imposing jumps in the displacement Δ, and

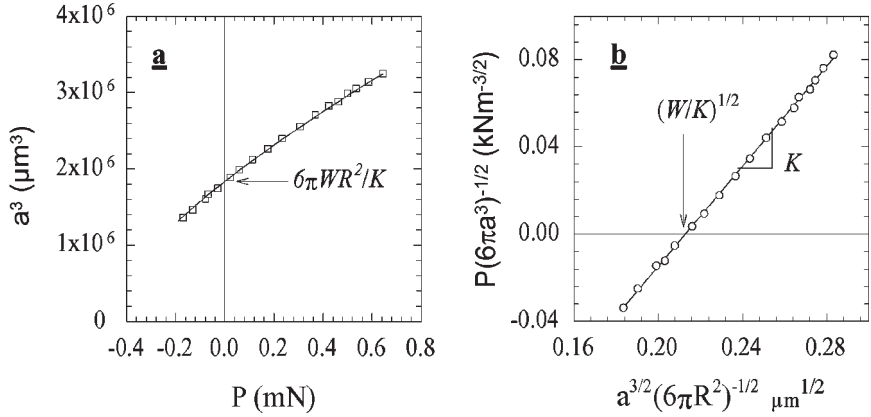

FIGURE 2 Typical loading curves for a silicone elastomer lens (0% MQ resin content) in contact with a silicon wafer covered with an evaporated gold layer and a dense self-assembled monolayer of alkyl thiol molecules with 20% of these chains bearing a COOH terminal function. Figure 2a gives the data in the usual JKR representation of Equation (1) and Figure 2b presents the same data in the linearized form of Equation (2).

monitoring a and P between each jump as a function of time. The adhesive strength is then deduced at each time through

$$G(t) = \frac{\left[P(t) - Ka(t)^3/R\right]^2}{6\pi K a(t)^3}. \tag{3}$$

The fracture velocity, V, can be calculated by the numerical derivative of $a(t)$.

It is then possible to construct the $G(V)$ curve. The simultaneous measurement of the displacement δ allows one to check for the validity of the JKR analysis, as a, δ, and P have to satisfy

$$\delta = \frac{a^2}{3R} + \frac{2P}{3aK}. \tag{4}$$

In Figure 3, a full cycle of loading and unloading is reported as an example. Figure 3a reports a^3 as a function of P, used to calculate G. The unloading steps, shown by the numbers 1 to 4, correspond to successive jumps with imposed displacements of the holder $\Delta = 5\,\mu m$. The unloading then proceeds between these jumps, at fixed Δ. In Figure 3b, the displacements δ are reported as a function of a, and the best fit to the JKR Equation 2 is the full line, in quite good agreement with the data points. No deviation due to finite-size effects is visible, because a thin ribbon (1 mm thick) of the same elastomer

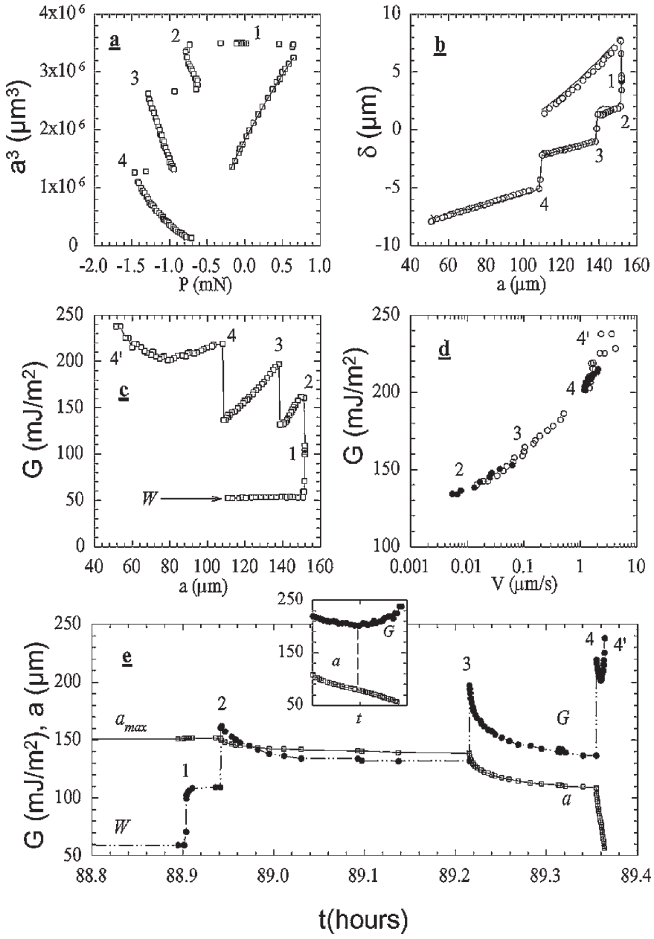

FIGURE 3 Typical loading and unloading cycle after a contact time of 90 h for the same system as in Figure 2. Curves a and b give, respectively, the evolution of the JKR parameters a, radius of contact, and δ, displacement at the center of contact, with, respectively, the load, P, and a. The different successive step-imposed displacements, Δ, are numbered from 1 to 4. The values of the adhesive strength, G, deduced from the JKR Equation (1) applied to the data of Figure 3a are reported in Figure 3c as a function of the contact radius. In Figure 3d, the same data are reported in terms of G *versus* the velocity of the advancing fracture during unloading [the velocity of the fracture is deduced by numerical time derivative of the monitored $a(t)$]. The different steps all contribute to a unique G(V) curve. In Figure 3e, the time evolutions of both G and a during the successive displacements steps have been reconstructed, showing clearly how the fracture velocity influences G, even if the average traction velocity is constant.

has been intercalated between the lens and the holder, following the procedure of Deruelle *et al*. [3]. In Figure 3c, G is reported as a function of a. During the compression, G is constant and equal to W. It is clear that the derivative $(\partial G/\partial a)_\Delta$ is positive for steps 2 and 3 and becomes negative during step 4. In Figure 3e, the evolution of G *versus* time during the full unloading cycle is reported. During step 1, the stored energy is insufficient ($110\,\mathrm{J/m^2}$) to produce a reduction of the contact area. After the second jump, a starts to decrease, and the fracture propagates with a velocity V, which decreases progressively in agreement with the sign of $(\partial G/\partial a)_\Delta$. The third step is similar and leads to a controlled decrease of the contact area. The evolutions of G and a with time during the fourth step are shown in the inset of Figure 3e. The minimum in G corresponds to the inflexion point in the $a(t)$ curve. After the inflexion point, the derivative $(\partial G/\partial a)_\Delta$ becomes negative, and the fracture accelerates until rupture takes place. In Figure 3d, the adhesive strength G is reported as a function of V. All unloading steps contribute to a unique $G(V)$ curve. This ensemble of data is a demonstration of the importance of a correct analysis of JKR experiments, especially because the fracture velocity may be quite different from the average velocity at which the elastomer lens is pulled off.

JKR under Zero Load

If the applied load is negligible, the JKR Equation (1) takes the simple form:

$$G = \frac{Ka^3}{6\pi R^2} \tag{5}$$

A simple measurement of the radius of contact, a, yields G provided the elastic modulus is known. The weight of a small PDMS lens with a radius $R = 1\,\mathrm{mm}$ is close to $10\,\mu\mathrm{N}$, while $Ka^3/R \approx 1000\,\mu\mathrm{N}$ for $a = 1200\,\mu\mathrm{m}$, $R = 1\,\mathrm{mm}$, and $K = 1\,\mathrm{MPa}$. This means that Equation (5) is a good approximation of what happens when the lens is allowed to evolve under its own weight. This means that $G(V)$ can also be monitored by first loading the lens under a constant load and then taking away the loading weight, and monitoring the evolution of a as a function of time, a procedure that has been widely used by several authors [7, 8]. In Figure 4, the system that we used to work that way is schematically presented. This procedure is particularly interesting when the system has to be investigated at very long contact times (days to months) for which the stability of the force sensors in normal JKR machine such as the one described in Figure 1 is insufficient.

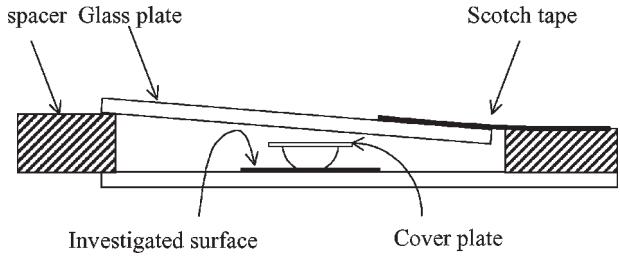

FIGURE 4 Schematic representation of the setup used to investigate long contact times in the so-called "zero-load JKR test." The lens is first loaded by pressing on it with the upper plate, during the chosen contact time. Then, the upper plate is taken up and the contact radius is monitored as a function of time while the only loading of the lens is its own weight, giving a constraint negligible in front of the elastic constraints in the system.

RESULTS

We have used the two versions of the JKR test with microlenses to investigate in detail the adhesive behavior of silicone elastomers containing variable amounts of MQ resins on acrylic adhesive layers.

We present here the results for two systems: silicone elastomer–silicone layer contact, which can be considered as a reference system with low adhesive strength, and silicone elastomer–molecular layer of an acrylic adhesive deposited on a rigid silicon-wafer surface. Reducing the thickness of the acrylic layer allows one to focus on the contribution to adhesive strength of the dissipations in the silicone elastomer, without mixing dissipations coming from both sides of the fracture plane. Because the incorporation of MQ resins in the silicone elastomer strongly affects the loss moduli, the real difficulty in comparing data for different MQ resin contents is to ensure that the mechanical tests are indeed correctly conducted, taking into account the appearance of very long tails in the relaxation time spectra of the elastomers with high MQ resin content. In particular, we found that it was not possible to deduce the surface energies of the elastomers with high resin content through the usual loading JKR procedure, because too-long relaxation times prevented the assumption of a fully relaxed contact within reasonable waiting times, in view of (1) the stability of the force sensor and (2) the possible evolution of interactions under contact (slow reorganization of the elastomer close to the interface to expose the resins to the new environment). Also, these long relaxation times made it difficult to find a reasonable range of pulling velocities, allowing one to ensure that during unloading low-enough velocities could be investigated to provide a direct determination of a

zero-velocity adhesive strength, G_0. We present how we first used the JKR analysis of static contacts to extract the work of adhesion, W, in silicone–silicone contacts. Then, in a second step, we used JKR unloading for silicone–silicone contacts to extract the dissipation functions, $\phi(V)$, of the different elastomers, as a function of the resin content. Finally, these dissipation functions have been used to provide an extrapolation to zero velocity of the fracture and a determination of G_0 as a function of the resin content in the case of silicone elastomers in contact with a thin layer of acrylic polymer.

Silicone–Silicone Contact

The JKR test under zero load has been used to characterize the surface energy of the silicone elastomers as a function of the MQ resin content, working with an elastomer lens put into contact with the same elastomer ribbon. To test the contact mechanics [Equation (5)], we choose to vary the radius of the small lenses, get rid of long relaxation times by working under zero load, and wait for long contact times to let the elastomer fully relax all viscoelastic stresses.

Elastomer–Elastomer Contact

Typical evolutions of the radius of the contact area, a, under zero load, as a function of the radius of curvature of the lens, are reported in Figure 5 for two compositions of MQ resins. The linear adjustment [Equation (5)] assuming that equilibrium is reached so that $G = W$ yields the values reported in Table 1 for W/K and K. The dispersion for the 40% composition is rather large (small contact area due to the large rigidity of the elastomer at high MQ resin content) and does not allow a precise determination of the surface energy. A better way would have been to work in liquids with varying surface tensions (for example water–methanol mixtures, which do not swell the elastomer), deduce the solid–liquid surface tension measuring the contact area under the liquid environment, and then extrapolate to $\gamma_{sl} = 0$ to obtain the critical surface tension of the solid in a way similar to what Whitesides and Chaudhury have done [3].

Silicone Elastomer–Grafted PDMS Layer Contact

In a second step, to characterize the dissipation function of the elastomers as a function of the MQ resin content, we investigated the unloading behavior for contacts between PDMS elastomers with various resin content and a reference surface made of a silicon wafer covered with a layer of grafted short PDMS chains. If the molecular weight of the grafted chains is smaller than the molecular weight

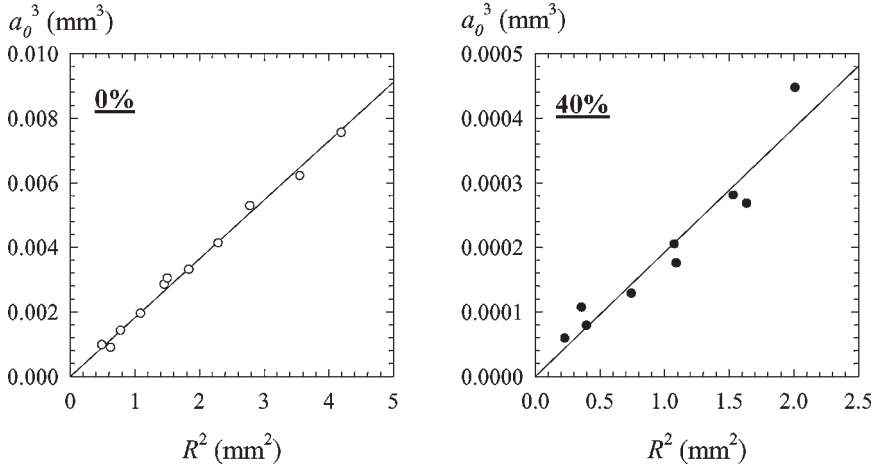

FIGURE 5 Relation between the radii of the contact area obtained long time after unloading and the radius of the lens for two MQ resin contents. The slope of the straight line gives W/K.

between entanglements (8 kg/mol for PDMS), such a surface is known to behave as an ideal surface with respect to both adhesion and friction [9–11], and almost no hysteresis is observed between loading and unloading against a 0% MQ resin content elastomer (see Figure 6). Then, the asymptotic value of the adhesive strength at vanishing fracture velocity, G_0, is equal to the thermodynamic work of adhesion, W. If the system follows the Gent and Schultz law [12], the dissipation function is given by $\phi(V) = (G - W)/W$. Zero-force JKR was used to span a large range in fracture velocities. The dissipation function can then be directly deduced from the measurements of the radius of

TABLE 1 Characteristics of Elastomers with 0% and 40% Resin Content, as Deduced from the Linear Adjustment of a^3 *versus* R in the JKR under Zero-Load Elastomer–Elastomer Contact Experiments Reported in Figure 5

Elastomer (%)	W/K nm	K (MPa, for $W = 43$ mN/m)
0	95.5 ± 2.3	0.45 ± 0.01
40	10.1 ± 1.6	4.26 ± 0.67

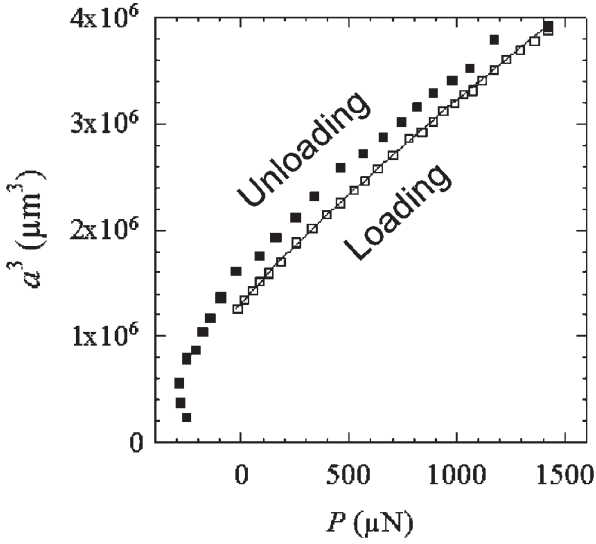

FIGURE 6 Loading and unloading curves for an elastomer with 0% MQ resin in contact with a dense grafted brush of PDMS 5 kg/mol. The G value is deduced from the loading curve, performed at a velocity $d\Delta/dt = 2\,\mu m/s$ is $45\,mJ/m^2$. The unloading is performed at the velocity $d\Delta/dt = -1\,\mu m/s$ gives $G = 55\,mJ/m^2$. The difference in the velocities can account for these different G values upon loading and unloading. No real hysteresis is measurable on the grafted 5-kg/mol PDMS layer.

the contact area, through $\phi(V) = (a^3 - a_{eq}^3)/a_{eq}^3$, with a_{eq} the measured radius of the contact area at equilibrium when the lens is just deposited on the substrate, without any other load than its own weight (*i.e.*, the equilibrium radius with $G = W$). In Figure 7, we have reported the evolution with time of the radius of the contact area normalized by the final radius, for various resin contents. The time necessary to reach equilibrium depends strongly on the amount of resins in the elastomer. Twenty minutes are needed to reach equilibrium in the case of the 40% elastomer, whereas only a few seconds are necessary for 0%. The data in Figure 7 can be translated in terms of velocity dependence of the adhesive strength, $G(V)$, as reported in Figure 8. For the two higher compositions in resin (30% and 40%) these curves can be described in terms of power laws for the dissipation function, $\phi(V) = (V/V^*)^n$, as shown in Figure 9. It is remarkable to notice that the exponent of the power law is similar for the two compositions, $n = 0.36 \pm 0.015$ and $V^* = 120 \pm 100\,\mu m/s$ for 30% and $n = 0.35 \pm 0.04$ and $V^* = 0.7 \pm 0.6\,\mu m/s$ for 40%.

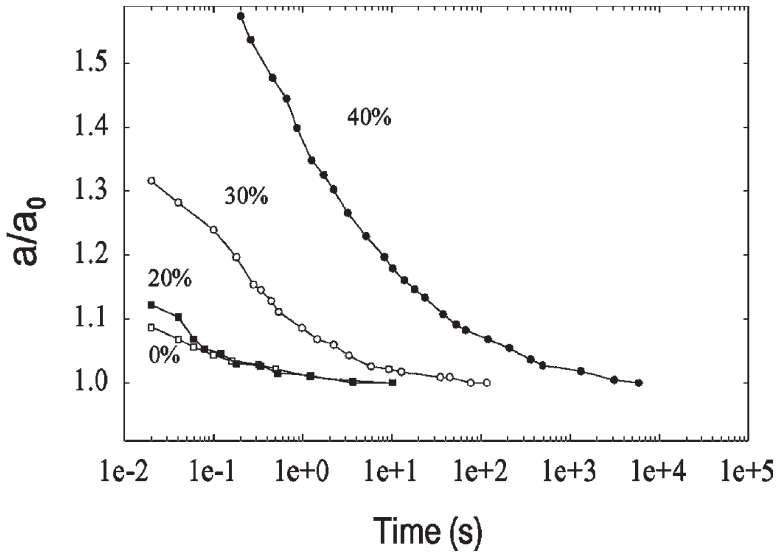

FIGURE 7 Typical evolution of the radius of the contact area, a, after unloading in a "zero-load JKR test" for elastomers with four different percentages of MQ resin content, in contact with a dense grafted 5-kg/mol PDMS layer.

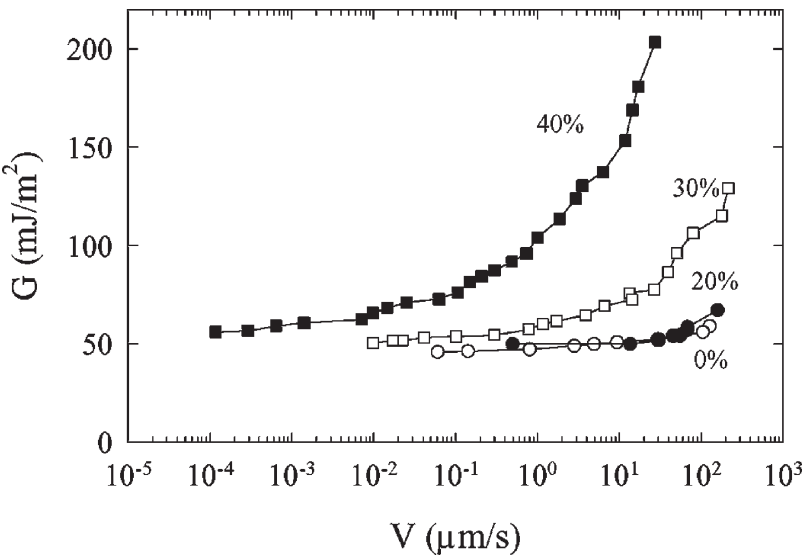

FIGURE 8 Corresponding evolutions of the adhesive strength, G, with the fracture velocity [obtained by numerical derivative of the $a(t)$ curves of Figure 7].

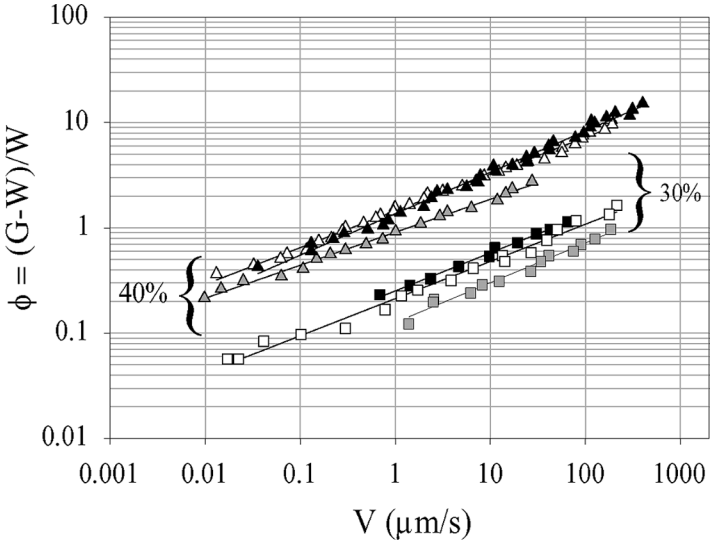

FIGURE 9 Dissipation functions, $\phi(V)$, for the two elastomers with 30% and 40% MQ resin content, when tested against the grafted 5-kg/mol PDMS layer. The three different curves for each composition of the elastomer correspond to measurements performed with three different lenses.

These evolutions of the dissipation functions with the fracture velocity are qualitatively similar to the evolutions of the loss modulus E'' with the frequency [1].

Silicon–Thin Acrylic Adhesive Layer Contact

To try to understand how interactions at the interface do affect the adhesive strength, without mixing with dissipation effects in the adhesive layer, we have investigated in a systematic manner the velocity dependence of the adhesive strength for the different elastomers put into contact with silicon wafers covered with a thin (30-nm) layer of a typical acrylic adhesive [a mixture of poly(2-ethylhexyl acrylate) and poly(methyl acrylate)] with 12% in weight of acrylic acid. Because of the very small thickness of the adhesive layer, one can expect that the dissipations when unloading come essentially from the elastomer. As W now is no longer known, we first need to measure it and then analyze the velocity dependence during unloading to determine the dissipation functions.

Loading Kinetics and Determination of the Dupré Adhesion Energy

In Figure 10, we have reported the loading curves obtained by compressing the elastomer lenses on the thin adhesive layer by successive increments of the displacement, $\Delta = 1\,\mu m$, every 30 s. The last point in each curve has been measured after a further waiting time of one night. The values of K and G deduced from Equation (2) are reported in Table 2. The values after one night appear larger than those deduced from the loading curve, and the difference is larger for the elastomer with the larger resin content. To better understand this effect, we have varied the loading velocity, using fixed increments in displacement of 1 μm, but varying the waiting time between two displacements. In Figure 11, we compare the results for elastomers with 0% and 40% resin content. The 0% appears insensitive to the loading rate, whereas the JKR curves for the 40% depend on the loading rate, with a weak decrease in the slope (K apparently goes from 6.5 to 6.27 MPa for a velocity decreased by a factor by 1000), whereas G appears more affected, varying from 16 to 41 mJ/m^2.

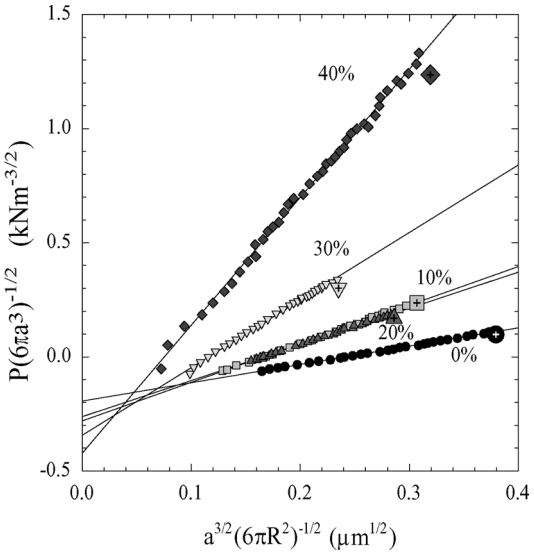

FIGURE 10 Loading curves obtained with lenses made of the four different MQ resin content elastomers in contact with a thin acrylic layer deposited on a silicon wafer. The compression was performed by step displacements of 1 μm every 30 s. The slope of the straight lines gives the rigidity modulus of each elastomer, and the value at $P = 0$ gives $(G/K)^{1/2}$. The last point on each curve corresponds to a contact time of one night.

TABLE 2 K and G Values Deduced from Adjustment of Equation 2 with the Data of Figure 10

Resin content (%)	K, MPa	G (apparent W), mJ/m^2	G after 1 night of contact, mJ/m^2
0	0.79 ± 0.01	46.5 ± 1.0	47.5 ± 1.0
10	1.69 ± 0.01	46.5 ± 1.0	47.7 ± 1.0
20	1.58 ± 0.01	42.6 ± 1.2	50.4 ± 1.4
30	2.95 ± 0.03	38.6 ± 1.5	51.0 ± 2.0
40	5.60 ± 0.05	32.0 ± 1.8	54.6 ± 3.0

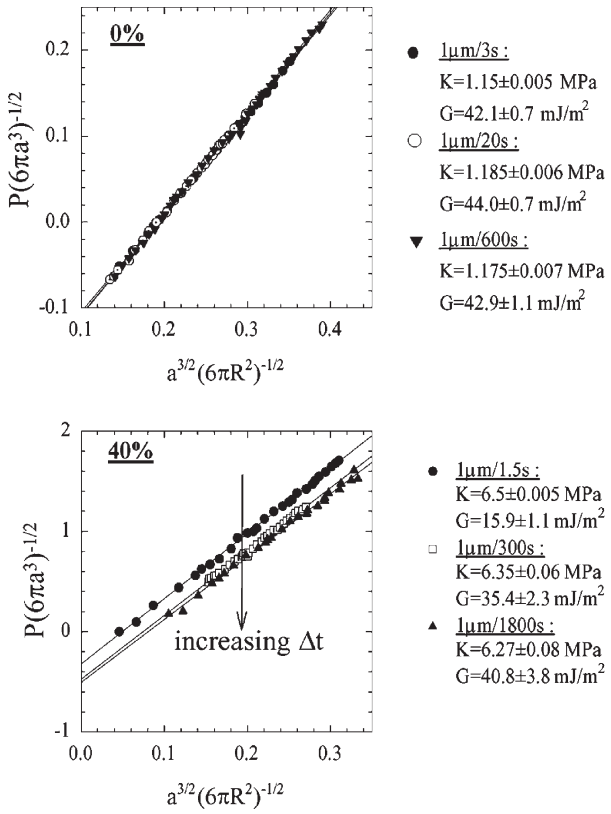

FIGURE 11 Loading curves as a function of effective loading velocity for two different MQ resin contents in the elastomer, in contact with a thin acrylic layer deposited on a silicon wafer. No obvious velocity effect can be detected for the 0% elastomer, whereas for the 40% elastomer G appears to increase when the effective velocity decreases.

In Figure 12, we report the evolutions of the contact area and of the force for a fixed imposed displacement step, Δ, for the same 40% elastomer. The radius increases continuously after the increment in displacement and needs several hours to stabilize, whereas the force reaches a plateau before starting to relax slightly at long times. Injecting the K value obtained for the slower loading rate ($K = 6.27$ MPa), one can translate these data in terms of adhesive strength as a

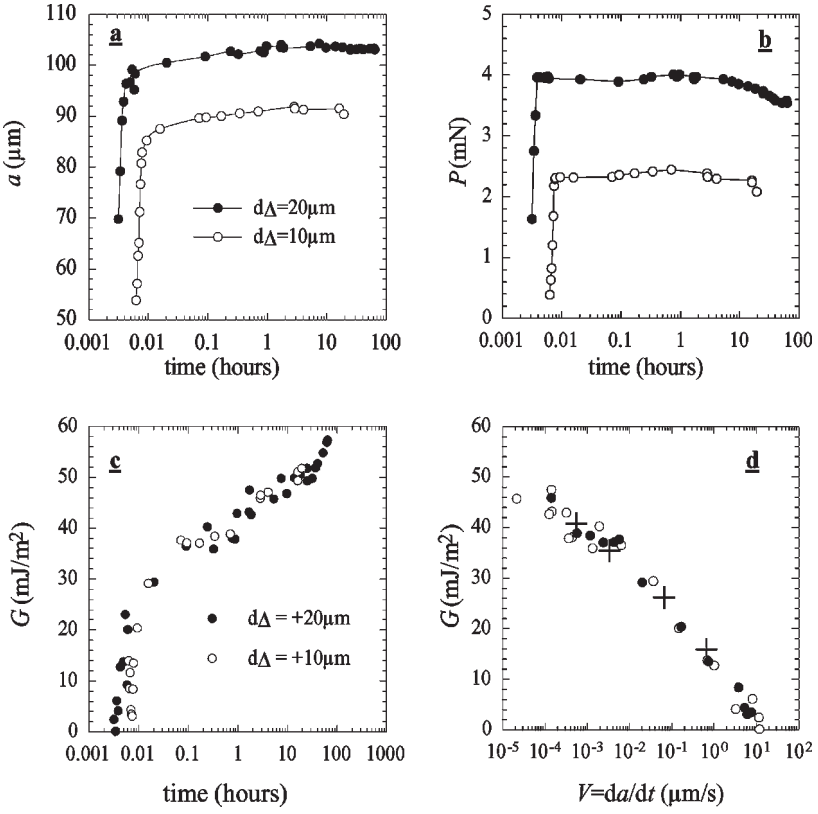

FIGURE 12 Evolutions with time of the radius of the contact area (a) and of the load (b) for two-step compressions ($\Delta = 20\,\mu$m and $10\,\mu$m) of an elastomer with 40% MQ resin content in contact with a thin layer of acrylic adhesive. The corresponding evolution with time of G (calculated with $K = 6.27$ MPa) is reported in Figure 12c. Figure 12d presents the velocity dependence of G, with the fracture velocity deduced from a numerical derivative of $a(t)$ shown in Figure 12a. The crosses in Figure 12d correspond to the G values obtained by compressing with step loading of different duration (Figure 11) and presented here as a function of the average advancing contact velocity.

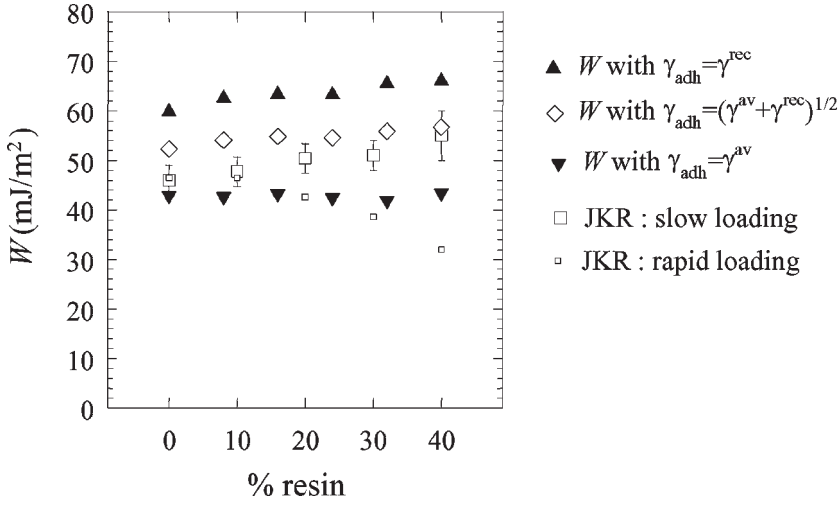

FIGURE 13 Work of adhesion for the elastomer–acrylic adhesive contact, as a function of the MQ resin content in the elastomer, as determined by direct measurements of the interfacial tensions (notice the large differences obtained when choosing advancing or receding values for the contact angles) or by the JKR test with a slow or a rapid loading. Deviations demonstrating the importance of taking correctly into account viscoelastic effects are clearly evidenced for the 40% elastomer, for which velocity effects lead to an underestimation of W.

function of the velocity, as shown in Figure 12d. At high velocity of the contact line, G tends toward zero. At very low velocity, one can admit that the measured G value is close to the zero velocity value, W (Figure 13).

It clearly appears from those experiments that to correctly extract a G value from JKR experiments, the viscoelasticity of the materials needs to be taken into account. The thermodynamic work of adhesion can be measured by the JKR test during the loading step, provided one takes care to proceed by loading steps and then wait for equilibrium, which can become quite difficult when the material develops long relaxation times, such as for the 40% elastomer.

Unloading Curves

Two parameters are important for the unloading step: the waiting time under load and the fracture velocity. The data *versus* these two parameters for the four resin contents are gathered in Figures 14–16.

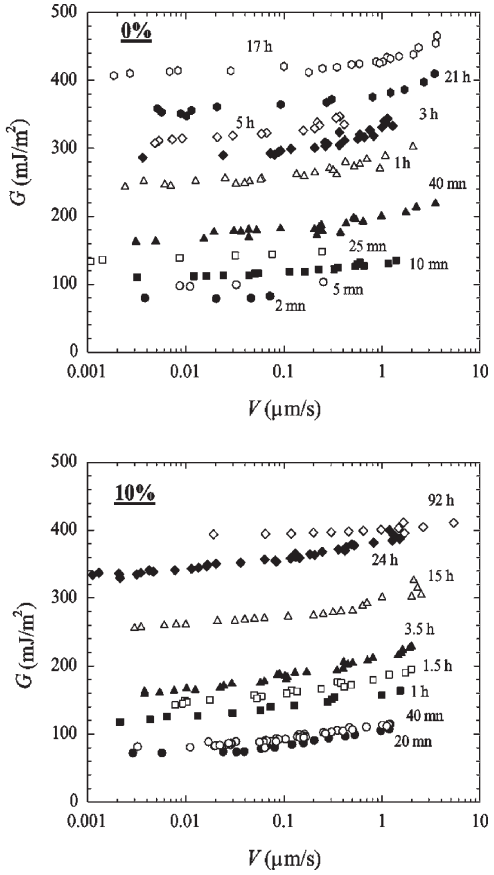

FIGURE 14 $G(V)$ curves obtained upon unloading for 0% and 10% MQ resin content elastomers in contact with a thin layer of acrylic adhesive deposited on a silicon wafer, for different contact times.

Clearly, the presence of the resin deeply affects the unloading behavior. Clearly, too, one cannot easily define a velocity below which velocity effects are negligible, within the experimentally attainable velocity range. To deduce from such data a zero velocity value of the adhesive strength, G_0, (which may strongly differ from W if interactions have developed under contact) we have assumed a Gent and Schultz behavior [12],

$$G - G_0 = G_0\phi(V) \tag{6}$$

and a dissipation function characteristic of the elastomer, *i.e.*, identical to that deduced from the investigation of the unloading

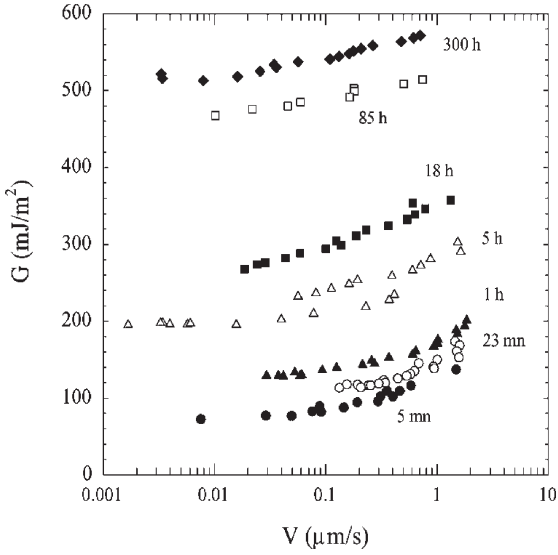

FIGURE 15 $G(V)$ curves obtained upon unloading for 20% MQ resin content elastomers in contact with a thin layer of acrylic adhesive deposited on a silicon wafer, for different contact times.

on the reference PDMS grafted layer. This second assumption could become questionable for a strain field inside the elastomer, that becomes very different from what it was for the elastomer–PDMS contact, which should not be the case here, with a rather moderate adhesion increase. The curves were thus fitted to Equation (6), imposing $n = 0.35$, and adjusting V^* to obtain a dissipation function close to that obtained on the PDMS layer. Such an adjustment is shown in Figure 17 for the 40% elastomer. From the corresponding G_0 values, one can investigate the kinetics of adhesive strength enhancement, as shown in Figure 18 for three resin contents. Three days appear necessary to saturate the adhesive strength for the 40%, whereas only a few hours are necessary in the case of the 0%. Surprisingly enough, the 20% reaches saturation after the 40%. For all three elastomers, the kinetics appears compatible with a $t^{1/2}$ law. These results are summarized in Figure 19, where the evolutions of G_0 with the resin content are reported at both short and long contact times. One can see that the adhesion energy tends to increase with the resin content, but in a nonmonotonous manner. A minimum in G_0 appears at short contact times for the 20%. This minimum disappears at long-enough contact times.

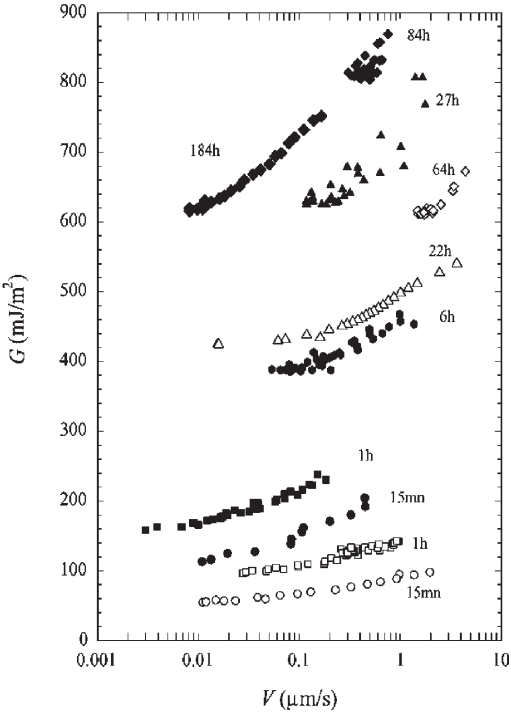

FIGURE 16 $G(V)$ curves obtained upon unloading for 30% (open symbols) and 40% (filled symbols) MQ resin content elastomers in contact with a thin layer of acrylic adhesive deposited on a silicon wafer, for different contact times.

The efficiency of the resin in terms of adhesion modulation, thus, appears as a complex competition between not yet fully understood kinetics effects.

We have shown that the resins only weakly affect the thermodynamic work of adhesion, W, as measured through JKR loading curves at equilibrium. From the unloading curves, we have shown that the resin content in the elastomer was able to deeply affect the limit at zero fracture velocity of the adhesive strength, G_0. The G_0 values appear to depend both on the contact time and on the resin content, in a nontrivial manner. At short contact times, G_0 increases as $t^{1/2}$. At long contact times, G_0 becomes independent of the contact time and increases linearly with the resin content, as shown in Figure 20. These G_0 values appear to follow but are enhanced by a factor of approximately 9, the thermodynamic work of adhesion values.

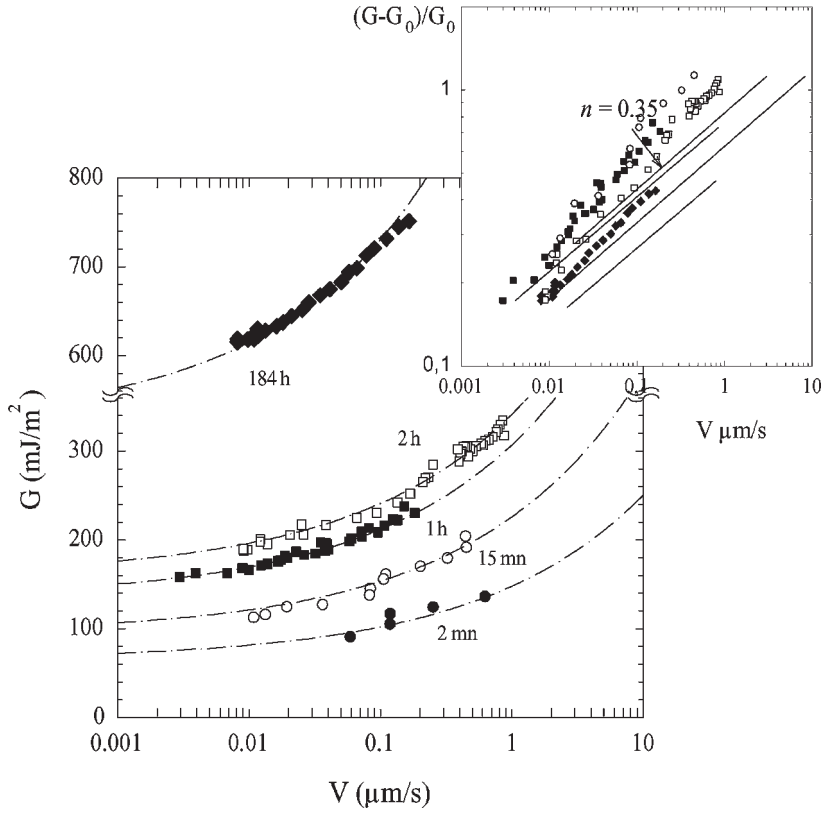

FIGURE 17 Extrapolation to zero velocity of the $G(V)$ curves for a 40% resin content elastomer in contact with a thin acrylic adhesive layer on a silicon wafer. In the inset, dissipation functions obtained by the fitting procedure (see text) are shown and can be compared with those of Figure 9.

Obviously, as soon as the fracture velocity is increased, a further enhancement develops, which is more pronounced for the elastomers with higher resin content.

CONCLUSIONS

By using complementary model systems, we have been able to decompose the complex adhesive behavior of PDMS elastomers containing various MQ resin contents in contact with acrylic adhesive thin layers in terms of thermodynamic work of adhesion, W, and limit at zero fracture velocity of the adhesive toughness, or adhesion energy, G_0, and velocity dependent adhesive strength, $G(V)$. For these systems, the

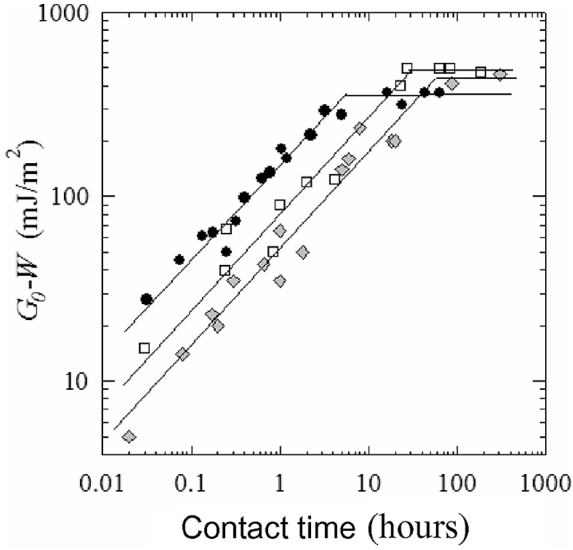

FIGURE 18 Adhesion hysteresis, $G_0 - W$, as a function of the contact time, for three compositions in MQ resins in the elastomer (0% filled discs; 20% filled diamonds; 40% open squares) in contact with a thin acrylic adhesive layer deposited on a silicon wafer. The lines suggest a $t^{1/2}$ dependence before saturation.

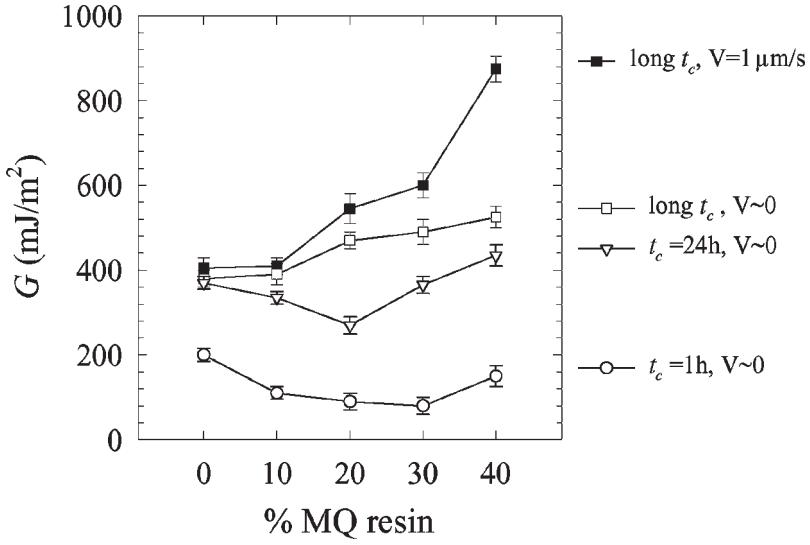

FIGURE 19 Evolution of G_0 as a function of the MQ resin content in the elastomer, for different contact times (open symbols). For comparison, data obtained upon unloading at 1 µm/s after long contact times are also reported (filled squares). The differences appear much more pronounced for the 40% elastomer.

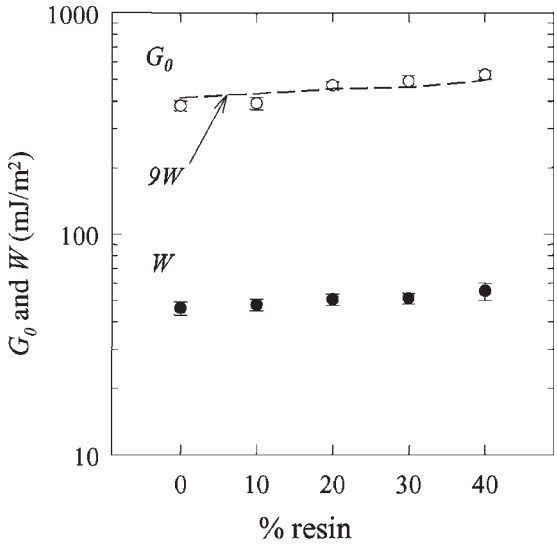

FIGURE 20 Comparison between the evolutions of the work of adhesion, W, and of the zero velocity fracture toughness, G_0, with the percentage of MQ resin content in the elastomer, for elastomer–thin acrylic layer contact. G_0 remains nine times as large as W.

thermodynamic work of adhesion is clearly smaller than the zero-velocity adhesion energy, implying specific dissipations in the immediate vicinity of the fracture front, such as, for example, chains in the acrylic layer, strongly interacting with the elastomer, and stretched and then extracted from the acrylic layer when the fracture propagates [13, 14]. These interactions are weakly sensitive to the resin content in the elastomer. The adhesive strength at finite velocity appears much more sensitive to the resin content and is markedly enhanced by the presence of MQ resins in the elastomer. We think that the enhancement of G_0 with resin content is the signature of increased interactions at the interface between the elastomer and the adhesive layer, allowing anchoring of acrylic chains at the interface under the contact with the elastomer. The effect of these interactions can be further enhanced through a coupling to velocities and dissipation effects as soon as the contact is broken at finite velocity, possibly through a stretching and extraction mechanism. To better trace the origin of such enhanced interactions, systematic experiments on complementary systems, with elastomers in contact with thiol-functionalized self-assembled monolayers so that interfacial interactions can be tuned, have been undertaken, and will be reported in a forthcoming paper. The reverse

systems, with acrylic elastomeric lenses in contact with PDMS thin layers or PDMS thick elastomers containing various MQ resin contents, have also been investigated to characterize the role of dissipations in the acrylic adhesive as a function of the MQ resin content in the PDMS elastomer. These experiments will also be reported in a third companion paper.

REFERENCES

[1] Amouroux, N., Petit, J., and Léger, L., *Langmuir* **17**, 6510–6517 (2001).
[2] Amouroux, N. and Léger, L., *Langmuir* **19**, 1396–1401 (2003).
[3] Chaudhury, M. K. and Whitesides, G. M., *Langmuir* **7**, 1013 (1991).
[4] Deruelle, M., Hervet, H., Jandeau, G., and Léger, L., *J. Adhes. Sci. Technol.* **12**(2), 225–247 (1998).
[5] Jonhson, K. L., Kendall, K., and Roberts, A. D., *Proc. R. Soc. A* **324**, 301–313 (1971).
[6] Maugis, D., *J. Mat. Sci.* **20**, 3041–3073 (1985).
[7] Vallat, M. F., Ziegler, P., Vondracek, P., and Schultz, J., *J. Adhes.* **35**, 95–103 (1991).
[8] Creton, C., Brown, H., and Shull, K. R., *Macromolecules* **27**, 3174–3183 (1994).
[9] Durliat, E., Hervet, H., and Léger, L., *Euro. Phys. Lett.* **38**, 383–388 (1997).
[10] Tardivat, C., Ph.D. Thesis, "Etude des mécanismes d'adhésion entre un élastomére et du verre. Renforcement de l'interface par une couche d'adhésif, ou par des chaînes connectrices," Université Paris XI (1998).
[11] Bureau, L. and Léger, L., *Langmuir* **20**, 4523–4529 (2004).
[12] Gent, A. and Schultz, J., *J. Adhes.* **3**, 281–294 (1972).
[13] de Gennes, P. G., *J. Phys. France* **50**, 2551–2562 (1989).
[14] Léger, L., Raphaël, E., and Hervet, H., *Adv. Polym. Sci.* **138**, 185–225 (1999).